Slot-DRA-Based Independent Dual-Band Hybrid Antenna for Wearable Biomedical Devices

AMJAD IQBAL[1,2], **(Student Member, IEEE), ABDULLAH J. ALAZEMI**[3], **(Member, IEEE), AND NAZIH KHADDAJ MALLAT**[4], **(Senior Member, IEEE)**

[1]Centre for Wireless Technology, Faculty of Engineering, Multimedia University, Cyberjaya 63100, Malaysia
[2]Department of Electrical Engineering, CECOS University of IT and Emerging Sciences, Peshawar 25000, Pakistan
[3]Department of Electrical Engineering, Faculty of Engineering and Petroleum, Kuwait University, Kuwait 13060, Kuwait
[4]College of Engineering, Al Ain University (AAU), Al Ain 64141, United Arab Emirates

Corresponding author: Abdullah J. Alazemi (aalazemi.ku@gmail.com)

ABSTRACT A hybrid dual-band antenna, consisting of an L-shaped radiating slot and a cylindrical dielectric resonator antenna (CDRA) is proposed, simulated and experimentally validated in this paper. The microstrip transmission line excites the fundamental mode (TM_{10}) of the slot that generates the lower frequency resonant band (2.4 GHz) and slot below the CDRA excites HEM_{11} mode of the CDRA to generate higher frequency band (5.8 GHz). The slot and CDRA modes are quasi-independent of each other and the resonant frequency of both modes can be adjusted quasi-independently. An equivalent circuit model of the independent modes and hybrid system is extracted to show the real behaviour of the modes and overall system. The on-body analysis of the antenna shows that the antenna is suitable for use in wearable biomedical devices.

INDEX TERMS On-Body antenna, slot antenna, hybrid antenna, dielectric resonator antenna, biomedical antenna, wearable antenna.

I. INTRODUCTION

With the swift development in telecommunication sector, there is an immense need for multi-standard, independently controllable, and compact radio frequency (RF) components. An antenna being an important component of the RF circuit is responsible for the transmission and reception of data [1], [2]. The design of a compact, multi-standard and independently band-controllable antenna is a challenging task. The slot antenna is considered as a best choice among the planar antennas because of its simple geometry. On the other hand, dielectric resonator antennas have drawn the focus of researchers because of its several advantages over the other antennas. A sufficient understanding of the DRA modes and excitation mechanism is required before designing a DRA. There are many techniques for exciting DRAs, such as microstrip feeding [3], slot feeding [4] and probe feeding [5]. The common method among all feeding mechanisms is the slot excitation, where the slot plays role to couple DR with the feed line. In the recent era, hybrid DRA has received considerable attention because of having advantages of compactness and multiple bands or wideband characteristics [4]. The hybrid DRAs are typically combination of a two

resonating structures with a common feeding mechanism, however, there are some literature where parasitic elements are used to generate extra modes in the DRA [4], [6]. There are certain limitations on the independent band control of the multi-mode DRA. The combination of DRA with other radiating structures is reasonable in order to control both bands independently. In [6], an LC resonator is loaded to a rectangular DRA, where the DRA operates at higher resonant frequency and LC resonator resonates at the lower frequency band, which makes a dual-band hybrid DRA. In [7], a conical DRA is excited by an eccentric ring slots, where the outer slot is resonating at lower resonant band, while the inner and outer slot excites the conical DRA at high resonant band, thus makes a dual-band hybrid DRA. A multiple band hybrid DRA is presented in [8], where the lower and second resonant band is generated with the aid of H-shaped monopole, while the higher resonant band is achieved by the combination of H-shaped monopole and rectangular DRA. The authors of [9], [10] designed a hybrid DRA, where slot beneath the DRA acts as a resonator as well as a feeder for the DRA. The antennas in [8]–[10] have high gain and radiation efficiency in the resonant bands, however, no band is independently controllable. A quasi-independently controllable dual-band hybrid antennas are presented in [11]–[13]. In [11], the DRA is fed with microstrip transmission line to excite the $HEM_{11\delta}$

The associate editor coordinating the review of this manuscript and approving it for publication was Mohsen Khalily.

mode and the radiating slot is optimized and placed on the ground plane to radiate at lower frequencies. In [12], an inductive slot resonates at the lower frequency band and feeds the DRA.

In recent times, wireless body area network (WBAN) has received considerable attention because of its vast applications in different sectors [14]. The importance of WBAN is further increased by the introduction of implantable devices for various applications such as capsule endoscopy [15], lead pacemakers [16], intra-oral tongue drive system [17], intracranial pressure monitoring [18], [19], and glucose monitoring [20]. An antenna is a vital component of the WBAN receiver. So far, numerous wearable antennas have been investigated for WBAN applications, however, there is a very limited study available on the DRAs and hybrid DRAs for WBAN. An ultra-wideband conical DRA is designed for WBAN in [14]. The antenna has a good performance in free space and on-body, however, the author did not discuss the backward radiations (specific absorption rate (SAR)). A textile DRA is investigated in [21], where the wideband response is achieved by truncating the DRA. A low-sized DRA for WBAN is investigated in [22], where miniaturization is accomplished by using multi-segment and a conducting wall. A single band textile DRA is also suggested in [23] for WBAN applications. All the aforementioned WBAN DRAs uses only one band or wideband operating frequency, however, it is always desirable for a wearable antenna to cover all possible industrial, scientific, and medical radio band (ISM band).

It is therefore, our proposed work is formulated, simulated and experimentally tested for both ISM bands (2.4 and 5.8 GHz). The major advantages of the proposed work are summarized as follows:

- To the best of our knowledge, this is the first ever dual-band hybrid DRA for WBAN, where the fundamental slot mode (TM_{10}) is excited to resonate at the lower ISM band (2.4 GHz) and $HEM_{11\delta}$ mode is excited in CDRA to get the high frequency ISM band (5.8 GHz).
- The proposed antenna is simulated and tested with full electronic packaging to visualize its performance in the real receiver/transmitter. To the best of our knowledge, no other DRAs have been investigated with electronic packaging.
- Each band of the hybrid antenna is independently controllable; the lower resonant band is controllable by adjusting the dimensions and position of the L-shaped slot while the higher resonant band can be controlled by adjusting the height, radius, and permittivity of the CDR.

II. DESIGN METHODOLOGY

The design process of the hybrid DRA is summarized as follows:

- An L-shaped slot antenna was designed for a 2.4 GHz in the first step. The equivalent circuit model was extracted to show the real behaviour of the circuit.
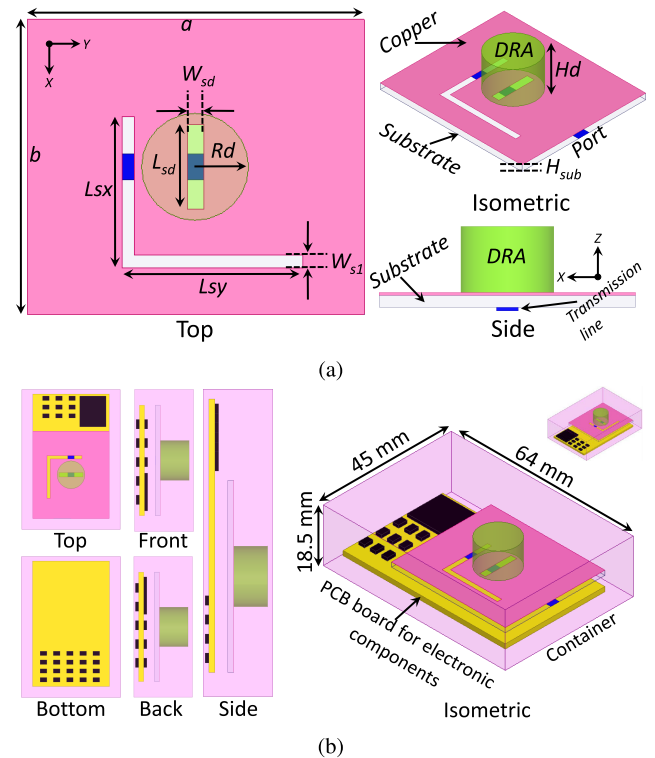

FIGURE 1. (a) Proposed slot-DRA based dual-band hybrid antenna [$Lsy = 21.5$, $Lsx = 18$, $W_{s1} = 1.5$, $L_{sd} = 11$, $W_{sd} = 2$, $Rd = 6.35$, $a = 40$, and $b = 35$, $Hd = 8$, and $H_{sub} = 1.6$ (unit = mm)], and (b) detail architecture of the wearable device.

- In the second step, a slot excited DRA was designed for a 5.8 GHz. The equivalent circuit model was extracted for DRA.
- A hybrid structure of slot-DRA was designed and optimized together in the third step. The position of the radiating slot and DRA was optimized for minimal coupling. An equivalent circuit model was also extracted for a hybrid system. The antenna was tested in the free space and in the vicinity of human body.
- In the last step, the antenna was modelled inside a container having different dummy electronics components to realize it in a quasi-real environment.

III. SLOT-DRA HYBRID ANTENNA DESIGN

The proposed slot and DRA based hybrid antenna is illustrated in Fig. 1a. The hybrid antenna comprises of an L-shaped radiating slot, a resonating DRA, and a non-resonating rectangular slot for DRA excitation. The non-radiating rectangular slot and radiating L-shaped slot are excited using a 50 Ω single microstrip transmission line. The hybrid antenna is designed on a commercially available 1.6 mm thicker FR-4 ($\epsilon_r = 4.4$, $\tan\delta = 0.020$) substrate. The optimized antenna parameters are listed in the caption of Fig. 1a. Fig. 1b shows device level quasi-receiver packaging, where the antenna is placed inside a box/container ($45 \times 64 \times 18.5$ mm³), considering the box/container as a receiver outer box. The receiver system comprises a PCB

X1	1.5
R_s	178.5 Ω
L_s	0.793 nH
C_s	6.3 pF
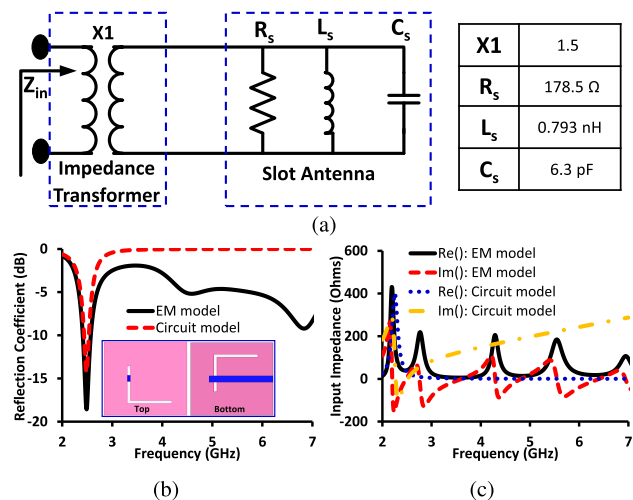
FIGURE 2. (a) Equivalent circuit model of the slot-antenna, (b) reflection coefficient comparison of the EM and circuit model, and (c) input impedance comparison of the EM and circuit model.

board where the electronic components are attached, our proposed antenna and the outer box/container. Initially, the dimensions of the radiating structures were calculated using the relations discussed in the literature. The proposed model uses two modes for dual band operation. The lower band is generated using the fundamental mode (TM_{10}) of the slot, while the upper band is generated using the $HEM_{11\delta}$ mode of the DRA. The hybrid antenna resonates at two frequencies, where the L-shaped radiating slot produces the lower frequency band and cylindrical DRA produces the upper resonant band. The detail and step-wise analysis of both modes and hybrid antenna are discussed in the following sections.

A. SLOT MODE OF THE ANTENNA: LOWER RESONANT BAND

The top and bottom view of the microstrip excited L-shaped slot antenna is shown in Fig. 2b. The width of the transmission line is calculated for 50 Ω impedance using Equation. (1) and (2) [24]. An L-shaped section from the ground plane is etched to make a half-wavelength radiating slot. The dimensions of the slot (length and width) were optimized to get the desired resonance at 2.4 GHz (ISM band). The initial dimensions of the slot were calculated using Equation. (3) [24].

$$\epsilon_{eff} = \frac{\epsilon_r + 1}{2} + \frac{\epsilon_r - 1}{2}\left(1 + 12\frac{h}{W}\right)^{-0.5} \quad (1)$$

$$Z = \frac{120\pi}{\sqrt{\epsilon_{eff}}}\left[\frac{W}{h} + 1.393 + 0.677ln\left(\frac{W}{h} + 1.444\right)\right]^{-1} \quad (2)$$

where ϵ_{eff} is the effective permittivity of the material, ϵ_r is the relative permittivity of the substrate, h is the thickness of the substrate and W is width of the transmission line.

$$L_{slot} = Lsx + Lsy = \frac{c}{2f_{res}}\left(\sqrt{\frac{\epsilon_r + 1}{2}}\right)^{-1} \quad (3)$$

where L_{slot} is the total length of the radiating slot, f_{res} is the resonant frequency generated by the radiating slot, c is the speed of light in air, and ϵ_r is the relative dielectric constant of the substrate.

The antenna resonated at 2.4 GHz in the slot mode with 10-dB bandwidth of 190 MHz (2.37–2.56 GHz) and fractional bandwidth of 7.8 %, as shown in Fig. 2b. An equivalent circuit model for the slot antenna was modelled, as illustrated in Fig. 2a. A 50 Ω microstrip transmission line is modelled as an impedance transformer, and the radiating slot is modelled as a parallel RLC resonant circuit [25], [26]. The equivalent circuit model was optimized in the Advanced Design System (ADS) and the optimized values are listed in Fig. 2a. The reflection coefficient of the circuit model and electromagnetic (EM) model is compared in Fig. 2b. We can see that the circuit model resonates at the same frequency as the EM model, however, there is a little mismatch in the bandwidth of both model. Additionally, the EM model has some dips in the out of band region because of the higher modes of the slot. But the circuit model has only one resonance as we modelled the circuit model for one resonance and we didn't consider the higher modes in our modelling. The input impedance of the EM model and circuit model is compared in Fig. 2c, which shows a reasonable agreement.

B. CDRA MODE OF THE ANTENNA: HIGHER RESONANT BAND

We chose CDR as a resonant structure for the high resonant band. We excited the CDR by etching a rectangular slot below it. The cylindrical shape of the DR was selected to easily excite the desired mode and to efficiently control the resonant frequency, by adjusting the radius and height of the CDR. A rectangular slot acts as an equivalent magnetic dipole, which results in exciting the HEM_{11} mode of the CDR. The initial dimensions of the CDR were calculated using Equation. (4) [27], [28]. The type of material and dimensions of the CDR was chosen to realize the desired bandwidth. The impedance bandwidth depends on permittivity and the aspect ratio of the CDR [29].

$$f_{HEM_{11\delta}} = \frac{(k_o Rd) \times c}{2\pi Rd} \quad (4)$$

and

$$k_o Rd = \frac{6.324}{\sqrt{\epsilon_r + 2}}\left[0.27 + 0.36\left(\frac{Rd}{2Hd}\right) + 0.02\left(\frac{Rd}{2Hd}\right)^2\right]$$

where k_o is wavenumber, Rd is radius of the CDR, Hd is radius of the CDR and c is the speed of light.

The CDRA resonated at 5.77 GHz with 10-dB bandwidth (fractional bandwidth) of 590 MHz (10.1 %) in the DRA mode. An equivalent circuit model was designed for the DRA mode, as shown in Fig. 3a. The non-resonating slot beneath the CDR is modelled as an RLC circuit. The non-resonating slot is coupled with a microstrip transmission line as well as CDR using an impedance transformer. The equivalent circuit model was optimized in the Advanced Design System (ADS)

X1	X2	R_s	L_s	C_s	R_dra	L_dra	C_dra
1.02	0.57	250 Ω	0.58 nH	0.66 pF	297 Ω	0.79 nH	1.62 pF

(a)

(b)

(c)
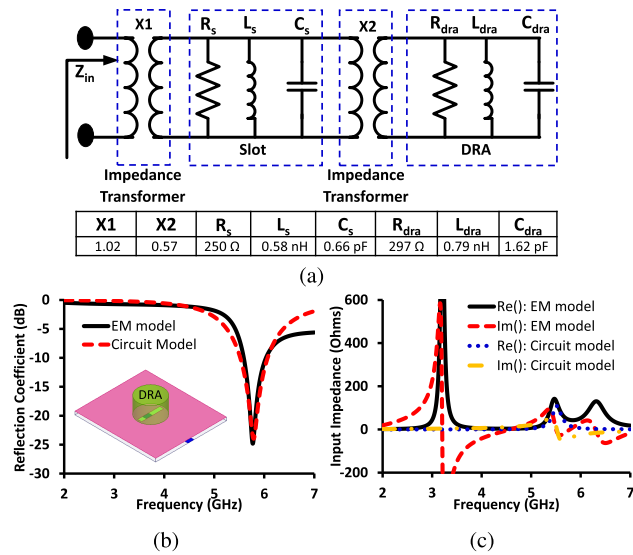
FIGURE 3. (a) Equivalent circuit model of the DRA, (b) reflection coefficient comparison of the EM and circuit model, and (c) input impedance comparison of the EM and circuit model.
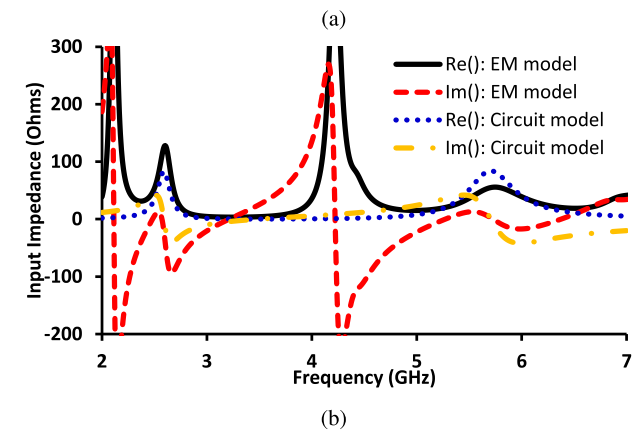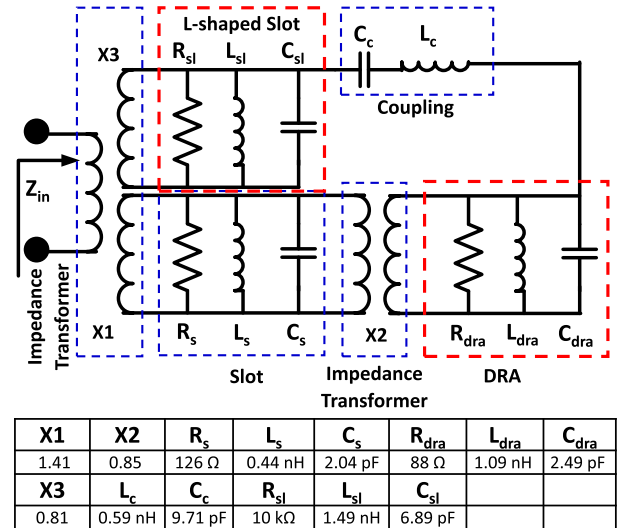
and the optimized values are listed in Fig. 3a. The reflection coefficient of the circuit model and the electromagnetic (EM) model is compared in Fig. 3b. We can see that the circuit model resonates at the same frequency as the EM model. The input impedance of the EM model and circuit model is compared in Fig. 3c, which shows a reasonable agreement.

C. HYBRID SLOT-DRA DESIGN

The DRA and slot antenna were separately investigated and both resonators were packed in such a way that they can be integrated with each other in the later stage. In this stage, both the resonators were packed within the same substrate, having a common ground and a common source. The position of both resonators was selected so as to have a minimal coupling effect on each other. The optimized hybrid antenna along with the detailed parameter dimensions are portrayed in Fig. 1a. The equivalent circuit model of the hybrid system is derived so as to see the real behaviour of the system. The L-shaped resonating slot, DRA, and slot beneath the DRA was modelled as an RLC circuit. The undesirable coupling between the radiating L-shaped slot and DRA was modelled as an LC circuit [30], [31]. The equivalent circuit model was optimized in the Advanced Design System (ADS) and the optimized values are listed in Fig. 4a. The input impedance of the EM model and the circuit model is compared in Fig. 4b, which shows a reasonable agreement.

D. ELECTRIC FIELD DISTRIBUTION

Electric field distribution of the antenna inside the device at 2.4 GHz and 5.8 GHz is illustrated in Fig. 5. The E-fields are concentrated on an L-shaped slot at 2.4 GHz and on the DRA at 5.8 GHz, which further confirms the operating mode of each band. It is evident from the Fig. 5 that the L-shaped slot is responsible for the lower resonant band and

X1	X2	R_s	L_s	C_s	R_dra	L_dra	C_dra
1.41	0.85	126 Ω	0.44 nH	2.04 pF	88 Ω	1.09 nH	2.49 pF

X3	L_c	C_c	R_sl	L_sl	C_sl		
0.81	0.59 nH	9.71 pF	10 kΩ	1.49 nH	6.89 pF		

(a)

(b)

FIGURE 4. (a) Equivalent circuit model of the slot-DRA based hybrid antenna, and (b) reflection coefficient comparison of the EM and circuit model.

(a)   (b)
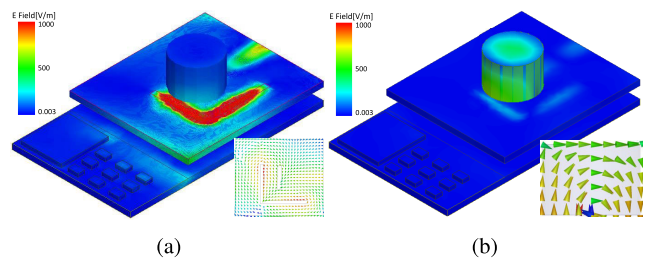
FIGURE 5. Electric field distribution of the antenna in the presence of the wearable device at (a) 2.4 GHz, and (b) 5.8 GHz.

CDR is responsible for the higher resonant band. We can also see from the Fig. 5 that the electronic packaging and 3-D container have negligible effects on the antenna. It is noticeable that a less amount of current is coupled with the electronic packaging, as shown in Fig. 5a-5b. Hence, it is confirmed from the discussion that the 3-D device and electronic packaging is not offering any detuning effects.

E. PARAMETRIC ANALYSIS

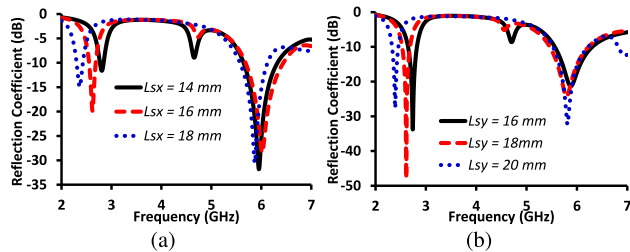As evident from Fig. 5 that the lower resonant band is generated because of an L-shaped slot and the higher resonant

FIGURE 6. Reflection coefficient of the antenna by varying (a) L_{sx}, and (b) L_{sy}.

FIGURE 7. Reflection coefficient of the antenna by varying (a) radius of the DRA (*Rd*) and (b) height of the DRA (*Hd*).

FIGURE 8. Specific absorption rate (SAR) (a) without the device, and (b) with the device.

band is generated by exciting an $HEM_{11\delta}$ mode in the CDRA. The desired performance of each band of the antenna was achieved through parametric analysis. We did the parametric analysis by varying the slot's parameters (L_{sx} and L_{sy}) and CDRA parameters (Hd and Rd).

1) SLOT LENGTH (L_{SX} AND L_{sy})

The lower resonant frequency of the antenna is quite reactive to the dimensions of the L-shaped resonating slot. The lower resonant frequency of the antenna shifted towards the lower frequency side by increasing the slot's dimensions (L_{sx} and L_{sy}). Fig. 6a shows the sensitivity of the resonant bands to the slot's dimension (L_{sx}). The antenna was simulated with three different values of L_{sx}. The lower resonant band of the antenna resonated at 2.82 GHz for $L_{sx} = 14$ mm, at 2.62 GHz for $L_{sx} = 16$ mm, and at 2.38 GHz for $L_{sx} = 18$ mm, while the higher band remained almost same for all values. We see that the lower resonant band shifted to the lower frequency by increasing the slot's length (L_{sx}) because L_{sx} is inversely related to the resonant frequency. In the same way reflection coefficient of the antenna was observed by sweeping the values of L_{sy} from 16 to 20 mm with a step size of 2 mm, as shown in Fig. 6b. The lower resonant band of the antenna resonated at 2.74 GHz for $L_{sy} = 16$ mm, at 2.61 GHz for $L_{sy} = 18$ mm, and at 2.39 GHz for $L_{sy} = 20$ mm, while the higher band remained almost the same for all values. We see that the lower resonant band shifted to the lower frequency by increasing the slot's length (L_{sy}) because L_{sy} is inversely related to the resonant frequency as defined in Equation. (3).

2) DRA DIMENSIONS, RADIUS(*RD*) AND HEIGHT (*Hd*)

It is evident from Fig. 5 that the higher frequency resonant band is generated by the DRA. The DRA is operating at $HEM_{11\delta}$ mode and the resonant frequency of the $HEM_{11\delta}$ mode is dependent on permittivity, radius (*Rd*) and height (*Hd*) of the DRA, as evident from Equation. (4). The higher resonant band of the antenna shifted from 5.88 to 5.41 GHz by changing *Rd* value from 5.85 to 7.35 mm. We see that the first resonant band of the antenna remained the same irrespective of *Rd* value, as shown in Fig. 7a. The impact of varying *Hd* on the reflection coefficient is portrayed in Fig. 7b. The higher resonant band of the antenna shifted from 5.74 to 5.5 GHz by changing *Hd* value from 7 to 13 mm. We see that the
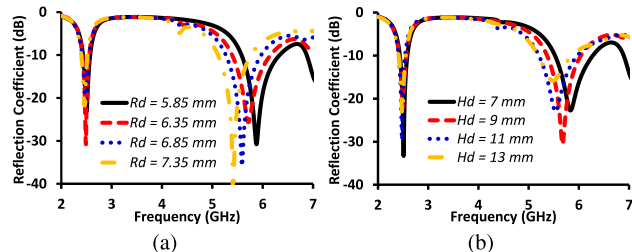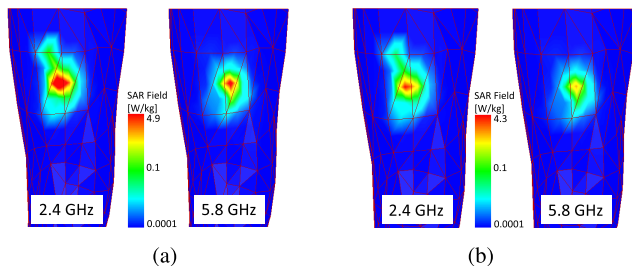
first resonant band of the antenna remained the same by any change in *Hd* value, as shown in Fig. 7b.

IV. SPECIFIC ABSORPTION RATE (SAR) ANALYSIS

The human body absorbs a portion of radiation when an antenna is placed in its nearby. These absorbed radiation increases temperature of the human body [32]. The intensity of the absorbed radiation is measured by the specific absorption rate (SAR) value. The SAR value can be calculated using the Equation. (5) [14]:

$$SAR = \frac{\sigma E^2}{\rho} \qquad (5)$$

where σ represents conductivity, E represent the electric field intensity, and ρ shows the mass density. We selected portion of the body instead of the whole phantom to reduce the simulation time. We calculated the SAR values in two cases (with and without the device) according to IEEE C95.1-2005. In the first case (without the device), we kept the antenna 3 mm away from the human leg and simulated the SAR value. In the second case (with device), we kept the device 2 mm away from the human body. Fig. 8 shows the SAR distributions in two cases. We see that the SAR value in the second case is relatively lower than the first case. The reason behind the lower SAR value in the second case is attributed to the extra electronic packaging PCB board below the antenna, which acts as a quasi-reflector and reduces backward radiation [33]. In the first case, the peak 10-g SAR values of 4.9 and 4.1 W/kg was observed for an input power of 1 W at 2.4 and 5.8 GHz, respectively. In the second case, the peak 10-g SAR values of 4.3 and 3.2 W/kg was observed for an input power of 1 W at 2.4 and 5.8 GHz, respectively. The proposed antenna exceed the SAR limits for the input
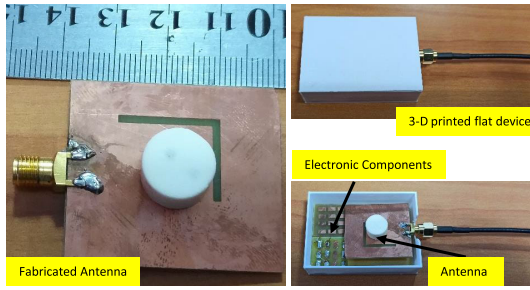
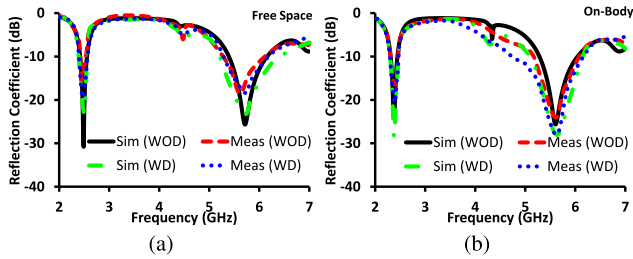**FIGURE 9.** Fabricated prototype of the slot-DRA based hybrid antenna.

FIGURE 10. Simulated and measured reflection coefficient of the antenna with the device (WD) and without the wearable device (WOD) (a) in free space (FS), and (b) in on-body (OB) case.

TABLE 1. Summary of the antenna's parameters (with the device = WD, and without the device = WOD).

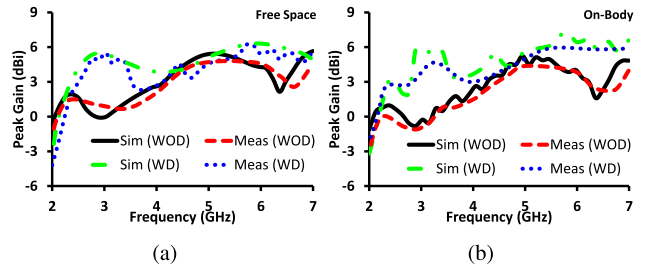| Paramters	Simulated/ Measured	Free Space		On-Body	
		WOD	WD	WOD	WD
Resonant Frequency (GHz)	Simulated	2.4	2.4	2.4	2.4
		5.8	5.79	5.78	5.78
	Measured	2.39	2.4	2.4	2.4
		5.76	5.78	5.78	5.78
Bandwidth (MHz)	Simulated	120	125	120	121
		650	674	647	673
	Measured	118	120	120	120
		639	653	710	800
Gain (dBi)	Simulated	2.01	4.2	0.97	3.1
		5.84	6.5	3.84	7.22
	Measured	1.93	4	0.55	2.99
		5.85	6.54	5.83	6.35
SAR (W/kg)	Simulated	–	–	4.9	4.3
		–	–	4.1	3.2

FIGURE 11. Simulated and measured peak gain of the antenna with the device (WD) and without the wearable device (WOD) (a) in free space (FS), and (b) in on-body (OB) case.

power of 1 W, however, input power of the wearable device must be in the range of mW [2]. Based on the SAR values of the proposed antenna, our antenna is safe if the input power is less than 408 mW.

V. RESULTS AND DISCUSSIONS

A prototype of the proposed model was fabricated using FR-4 substrate ($\epsilon_r = 4.4$, $\tan\delta = 0.020$) based on the optimized values of the antenna. The radiating L-shaped slot and rectangular slot on the ground plane of the substrate and microstrip transmission line were created using the chemical etching process. A cylindrical DR of alumina ceramic material having $\epsilon_r = 9.8$, radius = 6.35 mm and height = 8 mm was fixed over a rectangular slot using a conductive glue. A container/box was designed using 3-D printing technology to test the antenna inside the container with other electronic components. The box/container was considered as a quasi-receiver. The container consists of electronic packaging and antenna. The proposed antenna was practically tested with and without a device. The s-parameters of the antenna were measured using a vector network analyzer and far-field parameters were measured using a signal generator, horn-antenna, and spectrum analyzer in the echo-free anechoic chamber. The horn antenna was fixed and the test antenna was rotated along $\phi = 0°$ and $\phi = 90°$ plane. The distance between the horn antenna and the test antenna was 2 meters for measuring the received power.

Fig. 10 compare the simulated and measured reflection coefficient of the antenna in free space and in vicinity of the body. We can see that there is no significant mismatch between the simulated and measured results, as shown

in Fig. 10. It is noticeable that bandwidth of the antenna in the higher band is improved in case of the device because of the cavity effect generated by the PCB board [34]. It is worth noticing that the antenna has reasonable return loss and bandwidth in case of on-body worn scenarios, as shown in Fig. 10b. The simulated and measured s-parameters are summarized in Table. 1.

Fig. 11 compare the simulated and measured peak gain of the antenna in free space and in vicinity of the human body. The peak gain was measured with and without considering antenna inside a device. The simulated and measured gains are summarized in Table. 1. We see that gain of the antenna is enhanced because of the addition of PCB board which acts as a quasi-reflector. It is well-known that majority of antennas radiate some unwanted backward radiations, which decrease the gain, efficiency and deteriorates the radiation pattern. Controlling backward radiations can enhance antenna parameters such as gain, directivity, and efficiency. It is obvious from the literature [35], [36] that electromagnetic (EM) waves get reflected when moving from one medium to another. The PCB board in the device below antenna acts as a quasi-reflector with this concept. The reflection mechanism is further explained using Fig. 12. Fig. 12 has five regions of different permittivities, where *A* is the
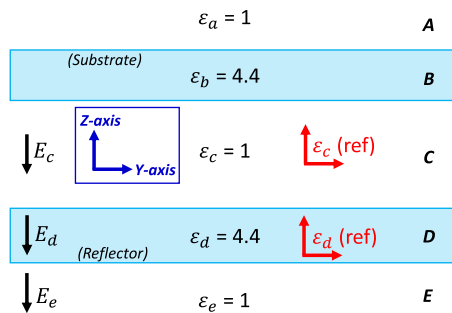
FIGURE 12. Reflection and incident wave in context to reflector.

FIGURE 13. Simulated and measured radiation pattern of the antenna with (WD) and without the wearable device (WOD) in free space (FS) and on-body (OB) (a) $\phi = 0°$ at 2.4 GHz, (b) $\phi = 90°$ at 2.4 GHz, (c) $\phi = 0°$ at 5.8 GHz (FS), and (d) $\phi = 90°$ at 5.8 GHz.

region above antenna's substrate with $\epsilon_a = 1$ and $tan\delta_a = 0$, B is the region inside antenna's substrate with $\epsilon_b = 4.4$ and $tan\delta_b = 0.02$, C is the region between antenna's substrate and PCB board (quasi-reflector) with $\epsilon_c = 1$ and $tan\delta_c = 0$, D is the region inside PCB board with $\epsilon_d = 4.4$ and $tan\delta_d = 0.02$, and E is the region below PCB board with $\epsilon_e = 1$ and $tan\delta_e = 0$. When a microstrip line is excited, some energy is used to excite $HEM_{11\delta}$ mode in CDRA and TM_{10} mode in the radiating slot. Apart from the energy that is used in coupling the radiating elements, some portion of the energy is released in region C and undergoes several reflections at C-D and D-E. The standardized equations in [37] can be used to evaluate the reflection and transmission of the EM waves at the medium interfaces. The ratio of reflected to incident wave is modelled as in Equation. (6) for the wave entering from region C to region D [35]–[37].

$$\left| \frac{E_c(ref)}{E_c} \right| = \left| \frac{\sqrt{(\epsilon_c - jtan\delta_c)/(\epsilon_d - jtan\delta_d)} - 1}{\sqrt{(\epsilon_c - jtan\delta_c)/(\epsilon_d - jtan\delta_d)} + 1} \right| \quad (6)$$

It is evident from Equation. (6) that the EM wave will undergoes reflection if $\epsilon_c \neq \epsilon_d$. It is also clear that a short-circuit situation will be created and a full wave will be reflected if the value of ϵ_d tends to infinity [38]. But in our case, both mediums have a finite values of permittivity. Moreover, the EM waves undergo a reflection at the interface of D-E and the ratio of reflected to incident wave can be formulated as Equation. (7).

$$\left| \frac{E_d(ref)}{E_d} \right| = \left| \frac{\sqrt{(\epsilon_d - jtan\delta_d)/(\epsilon_e - jtan\delta_e)} - 1}{\sqrt{(\epsilon_d - jtan\delta_d)/(\epsilon_e - jtan\delta_e)} + 1} \right| \quad (7)$$

It is clear from Equation. (7) that the EM wave will undergoes reflection if $\epsilon_d \neq \epsilon_e$, hence some of the waves will travel to region E and some will reflect to region D. The transmitted energy to region D or E can be calculated from Equations. (8)-(9).

$$\left| \frac{E_d}{E_c} \right| = \left| \frac{2}{\sqrt{(\epsilon_c - jtan\delta_c)/(\epsilon_d - jtan\delta_d)} + 1} \right| \quad (8)$$

$$\left| \frac{E_e}{E_d} \right| = \left| \frac{2}{\sqrt{(\epsilon_d - jtan\delta_d)/(\epsilon_e - jtan\delta_e)} + 1} \right| \quad (9)$$

The aforementioned equations are suffice to validate our claim that the PCB board acts as a quasi-reflector and increases gain of the antenna in both bands.
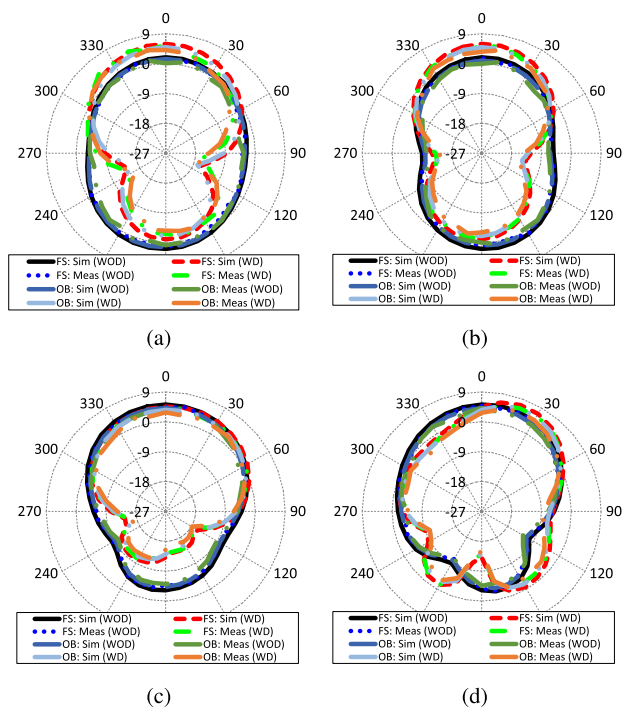
The radiation pattern of the antenna was measured in free space as well as in on-body worn scenario with and without considering the antenna in a device, and the results are compared with simulated one in Fig. 13. We see that the simulated results are in good accordance with the measured one. Also, it is worth noticing that the antenna performs well in the device as well as in vicinity of the human body. The proposed antenna's radiation pattern is somehow omni-directional at 2.4 GHz in both principal planes ($\phi = 0°$ and $\phi = 90°$). The introduction of PCB board below the antenna converts the omni-directional radiation to a quasi-directional pattern because of quasi-reflector behaviour of the PCB board. We can see that in both planes ($\phi = 0°$ and $\phi = 90°$), the backward radiation is reduced and the maximum radiations are at the broadside direction, as shown in Figs. 13a-13b. The antenna radiates like a conventional $HEM_{11\delta}$ mode at the higher resonant band (5.8 GHz). Fig. 13c illustrates the radiation pattern of the antenna in $\phi = 0°$ at 5.8 GHz. We see that radiation pattern is maximum at the broadside direction ($\theta = 30° - -330°$) and has low backward radiation. Moreover, the backward radiations were further reduced by keeping a PCB board below the antenna, as shown in Fig. 13c. Fig. 13d illustrate the radiation pattern of the antenna in $\phi = 90°$ at 5.8 GHz. It is noticeable that the radiation pattern is diverted a bit from $\theta = 0°$ to $\theta = 30°$, by keeping a PCB board below the antenna.

A comparison table (Table. 2) is included at the end of the discussion to show the advantages of our design. We see that our antenna is compact than other antennas

TABLE 2. Comparison of the proposed work with other hybrid antennas.

Ref.	Size ($*\lambda_1^2$)	Independently Controllable	Bandwidth (MHz)	Gain (dBi)	SAR (W/kg)
[4]	1.2×1.2	Yes	600	4.9	–
			500	5.3	–
[6]	1.15×1.15	Partially	140	6.25	–
			170	6.35	–
[8]	0.63×0.63	No	180	1.6	–
			480	2.34	–
			1310	4.79	–
[9]	0.83×0.83	No	860	7	–
			340	1.5	–
[11]	0.66×0.66	Partially	140	4.3	–
			400	3.8	–
[12]	0.97×0.97	Partially	312	4.7	–
			231	5.6	–
[13]	2.51×2.51	Partially	110	5.02	–
			320	4.09	–
[14]	0.12×π	–	1600	NA	NA
This Work	0.67×0.58	Yes	120	2.01	4.9
			650	5.84	4.1
*λ_1 is the guided wavelength at first resonant band.					

except [8], however, the resonant bands of [8] are independently non-controllable nor the antenna is tested for on-body communication. Moreover, the gains of [8] are lower than our proposed antenna. Our antenna is fully independently controllable, while other designs are either not or partially controllable. It is worth noticing that our designed antenna was tested on the device level, considering the device as a wearable receiver.

VI. CONCLUSION

A low-profile, dual-band hybrid antenna using an L-shaped slot and cylindrical DR as a resonator has been proposed in this paper. The parametric study confirms that the proposed antenna is independently controllable: the lower band is controllable using L-shaped slot's dimensions and higher resonant band is controllable using DR parameters (radius and height). A reliable equivalent circuit model has been presented for the individual resonators and hybrid antenna. The suitability of the antenna for biomedical devices is confirmed by embedding the antenna in a dummy biomedical receiver and by analyzing the SAR value in the device, and without the device. We found that the PCB board below the antenna acts as a reflector, results in increasing the gain, reducing the backward radiation, and reducing the SAR.

REFERENCES

[1] C. Zebiri, D. Sayad, I. Elfergani, A. Iqbal, W. F. Mshwat, J. Kosha, J. Rodriguez, and R. Abd-Alhameed, "A compact semi-circular and arc-shaped slot antenna for heterogeneous RF front-ends," *Electronics*, vol. 8, no. 10, p. 1123, 2019.

[2] A. Iqbal, A. Smida, L. F. Abdulrazak, O. A. Saraereh, N. K. Mallat, I. Elfergani, and S. Kim, "Low-profile frequency reconfigurable antenna for heterogeneous wireless systems," *Electronics*, vol. 8, no. 9, p. 976, 2019.

[3] S.-J. Guo, L.-S. Wu, K. W. Leung, and J.-F. Mao, "Microstrip-fed differential dielectric resonator antenna and array," *IEEE Antennas Wireless Propag. Lett.*, vol. 17, no. 9, pp. 1736–1739, 2018.

[4] A. Iqbal, A. Bouazizi, S. Kundu, I. Elfergani, and J. Rodriguez, "Dielectric resonator antenna with top loaded parasitic strip elements for dual-band operation," *Microw. Opt. Technol. Lett.*, vol. 61, no. 9, pp. 2134–2140, 2019.

[5] J. Iqbal, U. Illahi, M. I. Sulaiman, M. M. Alam, M. M. Su'ud, and M. N. M. Yasin, "Mutual coupling reduction using hybrid technique in wideband circularly polarized MIMO antenna for WiMAX applications," *IEEE Access*, vol. 7, pp. 40951–40958, 2019.

[6] A. Sharma, A. Sarkar, A. Biswas, and M. J. Akhtar, "Compact dual-band hybrid dielectric resonator antenna loaded with magnetic-LC resonator," *J. Electromagn. Appl.*, vol. 32, no. 10, pp. 1298–1305, 2018.

[7] Q. Rao, T. A. Denidni, and A. R. Sebak, "A new dual-frequency hybrid resonator antenna," *IEEE Antennas Wireless Propag. Lett.*, vol. 4, pp. 308–311, 2005.

[8] A. Gupta and R. K. Gangwar, "Hybrid rectangular dielectric resonator antenna for multiband applications," *IETE Tech. Rev.*, to be published, doi: 10.1080/02564602.2019.1565961.

[9] A. Sharma, G. Das, and R. K. Gangwar, "Dual-band circularly polarized hybrid antenna for WLAN/WiMAX applications," *Microw. Opt. Technol. Lett.*, vol. 59, no. 10, pp. 2450–2457, 2017.

[10] R. Kumari and R. K. Gangwar, "Circularly polarized slot-coupled square dielectric resonator antenna for WLAN applications," *Microw. Opt. Technol. Lett.*, vol. 60, no. 11, pp. 2787–2794, 2018.

[11] H. M. Chen, Y. K. Wang, Y. F. Lin, S. C. Lin, and S. C. Pan, "A compact dual-band dielectric resonator antenna using a parasitic slot," *IEEE Antennas Wireless Propag. Lett.*, vol. 8, pp. 173–176, 2009.

[12] Y.-F. Lin, H.-M. Chen, and C.-H. Lin, "Compact dual-band hybrid dielectric resonator antenna with radiating slot," *IEEE Antennas Wireless Propag. Lett.*, vol. 8, pp. 6–9, 2008.

[13] Y. Ding and K. W. Leung, "On the dual-band DRA-slot hybrid antenna," *IEEE Trans. Antennas Propag.*, vol. 57, no. 3, pp. 624–630, Mar. 2009.

[14] Y. Li, Z. Lu, and L. Yang, "CPW-fed slot antenna for medical wearable applications," *IEEE Access*, vol. 7, pp. 42107–42112, 2019.

[15] M. S. Miah, A. N. Khan, C. Icheln, K. Haneda, and K.-I. Takizawa, "Antenna system design for improved wireless capsule endoscope links at 433 MHz," *IEEE Trans. Antennas Propag.*, vol. 67, no. 4, pp. 2687–2699, Apr. 2019.

[16] S. M. Asif, A. Iftikhar, B. D. Braaten, D. L. Ewert, and K. Maile, "A wideband tissue numerical model for deeply implantable antennas for RF-powered leadless pacemakers," *IEEE Access*, vol. 7, pp. 31031–31042, 2019.

[17] M. Zada and H. Yoo, "Miniaturized dual band antennas for intra-oral tongue drive system in the ISM bands 433 MHz and 915 MHz: Design, safety, and link budget considerations," *IEEE Trans. Antennas Propag.*, vol. 67, no. 9, pp. 5843–5852, Sep. 2019.

[18] A. Basir and H. Yoo, "A stable impedance-matched ultrawideband antenna system mitigating detuning effects for multiple biotelemetric applications," *IEEE Trans. Antennas Propag.*, vol. 67, no. 5, pp. 3416–3421, May 2019.

[19] S. A. A. Shah and H. Yoo, "Scalp-implantable antenna systems for intracranial pressure monitoring," *IEEE Trans. Antennas Propag.*, vol. 66, no. 4, pp. 2170–2173, Apr. 2018.

[20] X. Y. Liu, Z. T. Wu, Y. Fan, and E. M. Tentzeris, "A miniaturized CSRR loaded wide-beamwidth circularly polarized implantable antenna for subcutaneous real-time glucose monitoring," *IEEE Antennas Wireless Propag. Lett.*, vol. 16, pp. 577–580, 2017.

[21] S. Mashhadi, Z. Wu, and L. Thamae, "Investigation of a wearable broadband textile dielectric resonator antenna," in *Proc. Loughborough Antennas Propag. Conf.*, 2010, pp. 349–352.

[22] M. S. Iqbal and K. P. Esselle, "A compact wideband dielectric resonator antenna for on-body applications," in *IEEE MTT-S Int. Microw. Symp. Dig.*, Dec. 2014, pp. 1–3.

[23] A. Iqbal and O. A. Saraereh, "Design and analysis of flexible cylindrical dielectric resonator antenna for body centric WiMAX and WLAN applications," in *Proc. Loughborough Antennas Propag. Conf. (LAPC)*, 2016, pp. 1–4.

[24] C. A. Balanis, *Antenna Theory: Analysis and Design*. Hoboken, NJ, USA: Wiley, 2016.

[25] U. Naeem, S. Bila, M. Thévenot, and E. Arnaud, "Design methodology for dual-band hybrid antennas with off-resonance loading," *IET Microw., Antennas Propag.*, vol. 11, no. 14, pp. 2077–2082, 2017.

[26] M. Alibakhshikenari, M. Khalily, B. S. Virdee, C. H. See, R. A. Abd-Alhameed, and E. Limiti, ''Mutual-coupling isolation using embedded metamaterial EM bandgap decoupling slab for densely packed array antennas,'' *IEEE Access*, vol. 7, pp. 51827–51840, 2019.

[27] A. Iqbal, A. Smida, O. A. Saraereh, Q. H. Alsafasfeh, N. K. Mallat, and B. M. Lee, ''Cylindrical dielectric resonator antenna-based sensors for liquid chemical detection,'' *Sensors*, vol. 19, no. 5, p. 1200, 2019.

[28] N. Yang, K. W. Leung, and N. Wu, ''Pattern-diversity cylindrical dielectric resonator antenna using fundamental modes of different mode families,'' *IEEE Trans. Antennas Propag.*, vol. 67, no. 11, pp. 6778–6788, Nov. 2019.

[29] A. Petosa, A. Ittipiboon, Y. M. M. Antar, D. Roscoe, and M. Cuhasi, ''Recent advances in dielectric-resonator antenna technology,'' *IEEE Antennas Propag. Mag.*, vol. 40, no. 3, pp. 35–48, Jun. 1998.

[30] M. Alibakhshikenari, B. S. Virdee, C. H. See, R. Abd-Alhameed, A. H. Ali, F. Falcone, and E. Limiti, ''Study on isolation improvement between closely-packed patch antenna arrays based on fractal metamaterial electromagnetic bandgap structures,'' *IET Microw., Antennas Propag.*, vol. 12, no. 14, pp. 2241–2247, 2018.

[31] A. Iqbal, O. A. Saraereh, A. Bouazizi, and A. Basir, ''Metamaterial-based highly isolated MIMO antenna for portable wireless applications,'' *Electronics*, vol. 7, no. 10, p. 267, 2018.

[32] A. Iqbal, A. Basir, A. Smida, N. K. Mallat, I. Elfergani, J. Rodriguez, and S. Kim, ''Electromagnetic bandgap backed millimeter-wave MIMO antenna for wearable applications,'' *IEEE Access*, vol. 7, pp. 111135–111144, 2019.

[33] S. K. K. Dash, T. Khan, B. K. Kanaujia, and N. Nasimuddin, ''Wideband cylindrical dielectric resonator antenna operating in $HEM_{11\delta}$ mode with improved gain: A study of superstrate and reflector plane,'' *Int. J. Antennas Propag.*, vol. 2017, Jul. 2017, Art. no. 2414619.

[34] F. Dong, L. Xu, W. Lin, and T. Zhang, ''A compact wide-band hybrid dielectric resonator antenna with enhanced gain and low cross-polarization,'' *Int. J. Antennas Propag.*, vol. 2017, Apr. 2017, Art. no. 6290539.

[35] R. F. Harrington, *Field Computation by Moment Methods*. Hoboken, NJ, USA: Wiley, 1993.

[36] R. K. Wangsness and R. K. Wangsness, *Electromagnetic Fields*, vol. 2. New York, NY, USA: Wiley, 1979.

[37] D. K. Cheng, *Field and Wave Electromagnetics*. London, U.K.: Pearson, 1989.

[38] Q. Rao, T. A. Denidni, and R. H. Johnston, ''Dielectric reflector backed aperture-coupled antennas for reduced back radiation,'' *IEEE Trans. Electromagn. Compat.*, vol. 48, no. 2, pp. 287–291, May 2006.

ABDULLAH J. ALAZEMI (M'15) received the B.S. degree in electrical engineering from Kuwait University, in 2010, and the M.S. and Ph.D. degrees in electrical and computer engineering from the University of California at San Diego, La Jolla, CA, USA, in 2013 and 2015, respectively. He joined the Department of Electrical Engineering, Kuwait University, where he is currently an Assistant Professor. His work focuses on tunable antennas and filters with RF-MEMS, multiband power dividers and couplers for advanced communication systems, and MM-wave to THz Quasi-optical systems.

NAZIH KHADDAJ MALLAT (M'07–SM'12) received the B.E. degree in electrical and electronics engineering from Lebanese University, Lebanon, in 2000, the master's degree from Ecole Nationale Supérieure des Télécommunications de Bretagne (ENSTB), France, in 2002, and the Ph.D. degree in telecommunications from the Institut National de la Recherche Scientifique (INRS), University of Quebec, Canada, in 2010. After his Ph.D. and until January 2012, he was a Postdoctoral Fellow with the Ecole Polytechnique de Montreal. The ''Fonds Québécois de la Recherche sur la Nature et les Technologies-FQRNT,'' a granting agency of the Quebec Government, has awarded him two prestigious scholarships for his Ph.D. studies, in 2008, and the Postdoctoral Research, from 2010 to 2011, thanks to his highest level of achievement. In 2013, he joined the College of Engineering, Al Ain University (AAU), United Arab Emirates (UAE) as an Assistant Professor, and was promoted to an Associate Professor, in 2019. His main research interests include passive microwave/millimeter-wave circuit, antennas, and telecommunications systems, where he authored or coauthored over 50 publications. He has acquired extensive teaching experience at undergraduate and graduate levels. He has effectively taught many courses, and their relevant practical elements in laboratories at multiple Montreal universities (ETS, TELUQ, and Ecole Polytechnique de Montreal). He was the Vice-Chair of the IEEE Montreal Section, from 2007 to 2008, the Membership Development Chair, from 2009 to 2010, and the Section Chair, from 2011 to 2012. He has also served in the Steering Committee of many IEEE international conferences. He was the Head of the Networks and Communication Engineering and Computer Engineering Department, from 2013 to 2017, the Deputy Dean of the College of Engineering, from 2014 to 2015 and September 2015 to March 2018. He has been the Director of the Quality Assurance and Institutional Research Center, since April 2018. He is the Founder of the IEEE AAU Student Branch and the IEEE UAE MTT-S Chapter (and later the IEEE UAE MTT-S & IM-S & AP-S Joint Chapter). He was the IEEE United Arab Emirates Technical Activities Coordinator, from 2015 to 2018, and the IEEE Region Eight Chapter Coordination Subcommittee Chair, from 2015 to 2016. He was the Organizing Committee Chair of three major events held at Al Ain University: The 1st IEEE International Workshop at AAU (February 2014), the 11th IEEE United Arab Emirates Student Day, in May 2016, and the 16th Mediterranean Microwave Symposium (MMS2016), in November 2016.

• • •

AMJAD IQBAL (S'18) received the degree in electrical engineering from COMSATS University, Islamabad, Pakistan, in 2012, and the master's degree in electrical engineering from the Department of Electrical Engineering, CECOS University of IT and Emerging Science, Peshawar, Pakistan, in 2018. He is currently pursuing the Ph.D. degree with the Faculty of Engineering, Multimedia University, Cyberjaya, Malaysia. He worked as a Lab Engineer with the Department of Electrical Engineering, CECOS University Peshawar, from 2016 to 2018. His research interests include printed antennas, flexible antennas, implantable antennas, MIMO antennas, dielectric resonator antennas, and synthesis of microwave components.